Magnetostructural Effect in the Multiferroic $BiFeO_3$-$BiMnO_3$ Checkerboard from First Principles

L. Pálová, P. Chandra, and K. M. Rabe

Department of Physics and Astronomy, Rutgers University, Piscataway, New Jersey 08854, USA

(Received 17 June 2009; published 20 January 2010)

Using first-principles calculations, we identify a magnetostructural effect in the $BiFeO_3$-$BiMnO_3$ nanocheckerboard that is not to be found in either the bulk parent compound or in $BiFeO_3$-$BiMnO_3$ superlattices with (001)-oriented Fe and Mn layers. The key role of the cation arrangement is explained by a simple model of the exchange coupling between cation spins, leading to magnetic frustration in the checkerboard. We also demonstrate that the atomic-scale checkerboard has a multiferroic ground state with the desired properties of each constituent material: polar and ferrimagnetic due to $BiFeO_3$ and $BiMnO_3$, respectively.

DOI: 10.1103/PhysRevLett.104.037202 PACS numbers: 75.80.+q, 75.70.Cn, 75.75.−c, 77.80.−e

There is great interest in finding new multiferroic materials with large magnetoelectric coupling. Advances in the synthesis of artificially structured materials have stimulated efforts to design new multiferroic heterostructures, with first-principles methods being an essential tool for the study of promising systems. In this Letter, we report the first-principles identification and characterization of an unusual heterostructure, a multiferroic atomic-scale 2D nanocheckerboard [1–4] of $BiFeO_3$-$BiMnO_3$, with properties that critically depend on the geometry and are not present in either bulk or (001)-oriented layered structures of the constituent materials. In particular, the 2D checkerboard geometry leads to magnetic frustration and to quasidegenerate magnetic states that could be tuned by an external perturbation that changes the crystal structure, such as epitaxial strain or electric field. This results in a novel magnetostructural effect, adding to previous examples of magnetostructural coupling such as bulk [5] and layered [6] manganites, epitaxial $EuTiO_3$ [7], and $EuSe/PbSe_{1-x}Te_x$ multilayers [8].

Our first-principles calculations are performed using density functional theory within the local spin-density approximation (LSDA) + U method as implemented in the Vienna *ab initio* simulation package VASP-4.6.34 [9]. We test the robustness of our results with two different implementations of the rotationally invariant LSDA + U version, the first as introduced by Liechtenstein [10] with $U_{\mathrm{Fe}} = U_{\mathrm{Mn}} = 5$ eV, $J_{\mathrm{Fe}} = J_{\mathrm{Mn}} = 1$ eV, and the second due to Dudarev [11], with $U^{\mathrm{eff}}_{\mathrm{Mn}} = 5.2$ eV, $U^{\mathrm{eff}}_{\mathrm{Fe}} = 4$ eV, where $U^{\mathrm{eff}} = U - J$. It has been shown that these U and J values match experimental data in bulk $BiFeO_3$ [12]; the value $U^{\mathrm{eff}} = 5.2$ eV has been used for previous bulk $BiMnO_3$ ground state calculations [13]. We use projector-augmented wave potentials (PAW) [14,15] and treat explicitly 15 valence electrons for Bi ($5d^{10}6s^26p^3$), 14 for Fe ($3p^63d^64s^2$), 13 for Mn ($3p^63d^54s^2$), and 6 for O ($2s^22p^4$). The cutoff energies for the plane wave basis set are 550 and 800 eV in the ionic relaxations and for subsequent self-consistent energy calculations, respectively. Gaussian broadening of the partial occupancies for each wave function is 0.05 eV. A Monkhorst-Pack k-point grid [16] is generated with density $4 \times 4 \times 4$ for the $(\sqrt{2} \times \sqrt{2} \times 1)a_0$ supercell and $4 \times 4 \times 2$ for the $(\sqrt{2} \times \sqrt{2} \times 2)a_0$ supercell. Ions are relaxed towards equilibrium positions until the Hellmann-Feynman forces are less than 10^{-3} eV/Å. The spontaneous polarization is calculated by the Berry phase method [17] with k-point mesh twice as dense as in the energy calculations.

We consider four formula units (perovskite cells), two each with Fe and Mn atoms on the B site, which we repeat periodically in space. For the planar checkerboard, we alternate Fe and Mn atoms to form pillars of the same composition as in Figure 1(ii); in the limit of the single unit-cell square considered here, the checkerboard structure is the same as that of a (110)-oriented superlattice. For

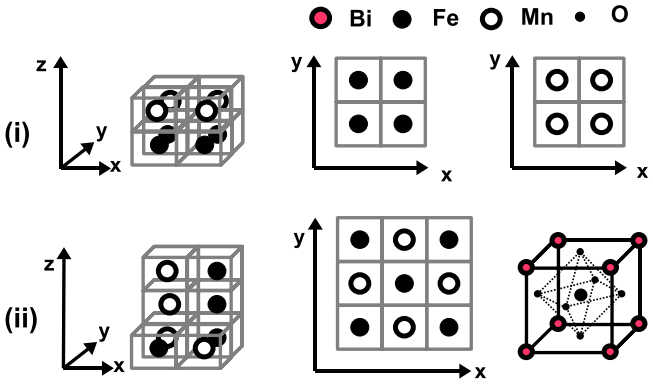

FIG. 1 (color online). (i) $BiFeO_3$-$BiMnO_3$ (001)-oriented layered superlattice with alternation of Fe/Mn planes. (ii) (left) $BiFeO_3$-$BiMnO_3$ checkerboard. Checkerboard ordering of Fe/Mn atoms in the (xy) plane, pillars of the same composition form along the z direction. (right) Ideal perovskite unit cell. Perovskite cells with Fe/Mn atoms on the B site repeat according to the checkerboard pattern (ii), or layered geometry (i).

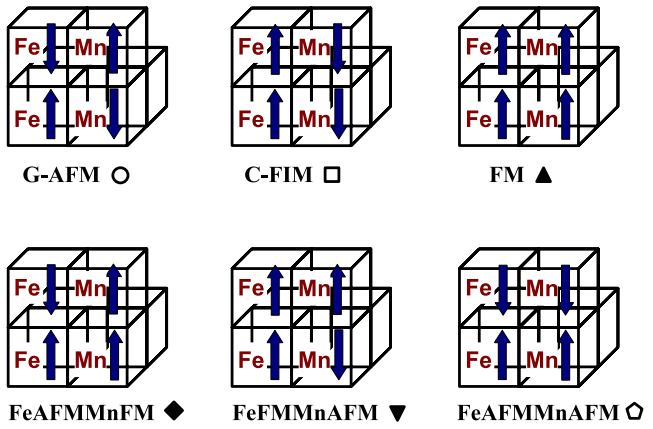

FIG. 2 (color online). From top left to bottom right: (i) *G*-AFM: rocksalt type antiferromagnetic (AFM) order; (ii) *C*-FIM: AFM order in horizontal planes, ferromagnetic (FM) order along Fe/Mn pillars; (iii) FM order; (iv) FeAFMMnFM: AFM order along Fe pillars, FM order along Mn pillars; (v) FeFMMnAFM: FM order along Fe pillars, AFM order along Mn pillars; (vi) FeAFMMnAFM: AFM order along Fe/Mn pillars, but FM order in horizontal planes.

the (001)-oriented superlattice, we alternate single unit-cell layers along z, as in Fig. 1(i). In both cases, the supercell is $\sqrt{2} \times \sqrt{2} \times 2$.

We study various collinear spin orderings of the magnetic Fe and Mn atoms. FeFM and FeAFM refer to ferromagnetic and antiferromagnetic ordering, respectively, for the Fe moments in the relevant structural component [pillar for the checkerboard, layer for the (001)-superlattice]; similarly MnFM and MnAFM describe the spin ordering of the Mn moments. In the checkerboard (see Fig. 2), this notation fully specifies the states considered. For the (001)-oriented superlattice, the remaining ambiguity is resolved as follows: FeAFMMnAFM magnetic order has AFM ordered Fe and Mn planes with FM order along the mixed Fe-Mn chains in the z direction, while *G*-AFM designates the case with AFM order along the mixed chains; similarly, FeFMMnFM has FM ordered Fe and Mn planes with AFM order, while FM designates the case with FM order, along the mixed chains.

First, to examine the effect of *B*-site cation geometry on the magnetic ordering, we show in Table I magnetic energies computed for the ideal perovskite structure. In the (001)-oriented superlattice and both bulk parent systems, the difference in energy between magnetic ground state (FeAFMMnFM in the superlattice, *G*-AFM in bulk $BiFeO_3$ and FM in bulk $BiMnO_3$) and the first alternative state is 0.10–0.14 eV/f.u.; this difference corresponds to a relatively large energy and we do not expect a transition to a different magnetic state. The highest energy magnetic states are more than 0.26 eV/f.u. apart. By contrast, in the checkerboard all magnetic states are quasidegenerate and are confined within the energetical window of 0.15 eV/f.u.; all are lower than the lowest states in the layered superlattice and the bulk. Indeed, the closest magnetic state to the FeAFMMnFM ground state is now only 0.022 eV/f.u. higher, making it much more plausible for a magnetic transition to occur.

The importance of the geometry of the cation arrangement in the magnetic ordering energies can be readily understood by considering a simple model of the exchange couplings between the cation spins. Since bulk $BiFeO_3$ and $BiMnO_3$ are known to be *G*-AFM and FM, respectively, the Fe-Fe and Mn-Mn interactions are taken as AFM and FM, respectively. In the (001)-oriented superlattice, each Fe(Mn) has four Fe(Mn) and only two Mn(Fe) nearest neighbors, so that the AFM ordering within the Fe layer and FM ordering within the Mn layers leaves only one ''unhappy'' Fe-Mn bond per cation. The FeAFMMnFM layered ground state is thus strongly favorable relative to any of the other magnetic orderings considered. In the checkerboard, the Fe pillars and Mn pillars are adjacent, so that even the most favorable configuration (AFM ordering in the Fe column and FM ordering in the Mn columns) leaves two ''unhappy'' Fe-Mn bonds per cation, and other magnetic orderings have similar proportions of ''unhappy'' Fe-Fe, Mn-Mn, and Fe-Mn bonds, making the energy cost relative to FeAFMMnFM relatively small. We will discuss this magnetic model more quantitatively elsewhere [18], where we will also relate it to the underlying electronic states.

TABLE I. Calculated total magnetic energies and energy differences in an ideal perovskite setting with lattice constant $a_0 = 3.893$ Å for various magnetic states in the checkerboard, layered superlattice, and bulk $BiFeO_3$ and $BiMnO_3$. Values of $U_{Fe} = U_{Mn} = 5$ eV and $J_{Fe} = J_{Mn} = 1$ eV are used in the first, and $U^{eff}_{Fe} = 4$ eV, $U^{eff}_{Mn} = 5.2$ eV with $U^{eff} = U - J$ in the second column.

Checkerboard magnetic state	E[eV/f.u.]	Layered superlattice magnetic state	E[eV/f.u.]	$BiFeO_3$ magnetic state	E[eV/f.u.]	$BiMnO_3$ magnetic state	E[eV/f.u.]
FeAFMMnFM	−35.04, −34.68	FeAFMMnFM	−35.11, −34.76	*G*-AFM	−34.23, −34.21	FM	−36.06, −35.40
	ΔE[eV/f.u.]		ΔE[eV/f.u.]		ΔE[eV/f.u.]		ΔE[eV/f.u.]
FeAFMMnFM	0.000, 0.000	FeAFMMnFM	0.000, 0.000	···	···	···	···
FM	0.022, 0.028	FM	0.111, 0.097	FM	0.360, 0.348	FM	0.000, 0.000
C-FIM	0.076, 0.113	FeFMMnFM	0.136, 0.143	*C*-AFM	0.115, 0.111	*C*-AFM	0.293, 0.365
FeAFMMnAFM	0.081, 0.084	FeAFMMnAFM	0.135, 0.137	*A*-AFM	0.223, 0.215	*A*-AFM	0.116, 0.139
G-AFM	0.114, 0.152	*G*-AFM	0.181, 0.219	*G*-AFM	0.000, 0.000	*G*-AFM	0.494, 0.621
FeFMMnAFM	0.119, 0.129	FeFMMnAFM	0.260, 0.257	···	···	···	···

Next we investigate the energetics of the structural distortion and its effect on the magnetic order. We use the Liechtenstein U and J parameters, as the Dudarev U^{eff} give similar results (see Table I). We consider structures generated by three typically unstable modes of the cubic perovskite [19]: the zone center polar Γ_4^-, the M_3^+ oxygen octahedron rotations (all rotations about a given axis in phase), and R_4^+ rotations (sense of rotations alternates along the rotation axis). We freeze in selected combinations of modes and optimize atomic displacements and lattice parameters in the resulting space groups. Before discussing the $BiFeO_3$-$BiMnO_3$ checkerboard, we look at the structural energetics of the bulk constituent materials, $BiFeO_3$ and $BiMnO_3$. We plot energies for various magnetic orderings in seven types of structural distortions of bulk $BiFeO_3$ in Fig. 3. Our calculation verifies the $R3c$ ground state: counterrotations of the oxygen octahedra (R_4^+) and polar ionic distortions (Γ_4^-) along the [111] axis are most energetically favorable [12,20]. The ground state structure has G-type AFM order and spontaneous polarization 90 $\mu C/cm^2$ along [111]. For all structural distortions considered, the lowest energy magnetic ordering is G-AFM.

We study the structural energetics of bulk $BiMnO_3$ in a similar way; the plotted energies are presented in Fig. 4. We find the lowest energy structure half-metallic and ferromagnetic, with the same $R3c$ symmetry as the ground state of $BiFeO_3$. This structure is not the monoclinic ground state $C2/c$ of bulk $BiMnO_3$ which has a larger unit cell than that considered here [21]. However, our calculation shows that it lies close to the ground state (only 43 meV/f.u. above the GS). For all structural distortions considered, the lowest energy magnetic ordering is FM.

In the (001)-oriented $BiFeO_3$-$BiMnO_3$ superlattice, we calculate magnetic energies for the rocksalt type G-AFM and FeAFMMnFM layered magnetic states in two structural distortions. For $R_4^+(y)$ and $\Gamma_4^-(y)$, we find $\Delta E = -0.504$ eV/f.u. for G-AFM and $\Delta E = -0.553$ eV/f.u. for FeAFMMnFM with respect to the FeAFMMnFM magnetic state in the ideal perovskite cell (see Table I). For $R_4^+([111])$ and $\Gamma_4^-([111])$, we find $\Delta E = -0.752$ eV/f.u. for G-AFM and $\Delta E = -0.761$ eV/f.u. for FeAFMMnFM. For both structural distortions considered, the lowest energy magnetic ordering is FeAFMMnFM.

Let us now look at the results for the structural energetics of the $BiFeO_3$-$BiMnO_3$ checkerboard. In Fig. 5, we present the energies for four different types of structural distortions; these show the lowest energies among a larger set of structures that we explored [18]. Not surprisingly, the R_4^+ and $\Gamma_4^-([111])$ ($R3c$) type of distortion is energetically the most favorable; it gives the $BiFeO_3$ ground state and the $BiMnO_3$ lowest energy structure. The $R3c$ symmetry is now broken due to pillar cation ordering and the space group of the ground state becomes $P1$; we use the notation c-$R3c$, where c designates "checkerboard", as a reminder of the origin of the distortions. As shown in the inset of Fig. 5, the two lowest magnetic states G-AFM and FeAFMMnFM, are only 2 meV/f.u. apart. The ground state of the checkerboard has the FeAFMMnFM magnetic order, where Fe spins are ordered antiferromagnetically along the Fe pillars, Mn spins are ordered ferromagnetically along the Mn pillars, reflecting "AFM" and "FM" nature of parent $BiFeO_3$ and $BiMnO_3$, respectively. A total magnetic moment $3.7\mu_B$ per Fe-Mn pair results from Mn chains. The FeAFMMnFM ground state is insulating with energy gap 0.88 eV, and we calculate a value of the polarization 62 $\mu C/cm^2$ pointing in the [0.85,0.85,1] direction. The ground state of the checkerboard is multiferroic, being ferroelectric and ferrimagnetic.

Finally, we discuss the sensitivity of the ordering of the magnetic levels to structural distortions. In the (001) superlattice, as in the parent compounds, the lowest energy magnetic ordering is unchanged by all structural distortions considered. In contrast, if we change the structural distortion in the checkerboard from the c-$R3c$ to the

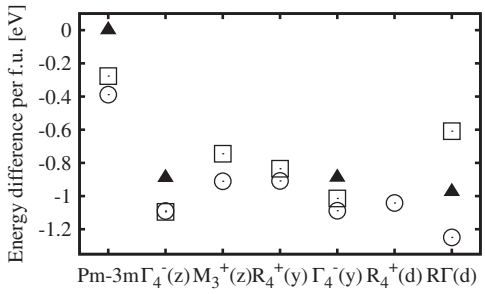

FIG. 3. Structural energetics of bulk $BiFeO_3$. Energy difference per perovskite cell (f.u.) for different magnetic orderings (see Fig. 2) and structural distortions: (1) $Pm\bar{3}m$: no distortion—ideal perovskite; (2) $\Gamma_4^-(z)$: polar distortion along z axis; (3) $M_3^+(z)$: + oxygen octahedra tilts about z axis; (4) $R_4^+(y)$: − oxygen octahedra tilts about y axis; (5) $R_4^+(y)$ and $\Gamma_4^-(y)$($R\Gamma(y)$): linear combination of (4) and (2) along y axis, relaxes back to polar $\Gamma_4^-(y)$ with zero tilting angle; (6) $R_4^+([111])$ ($R_4^+(d)$): − oxygen octahedra tilts about [111] axis; (7) $R_4^+([111])$ and $\Gamma_4^-([111])$ ($R\Gamma(d)$): linear combination of (6) and (2) along [111] (d), where d refers to the cube diagonal direction.

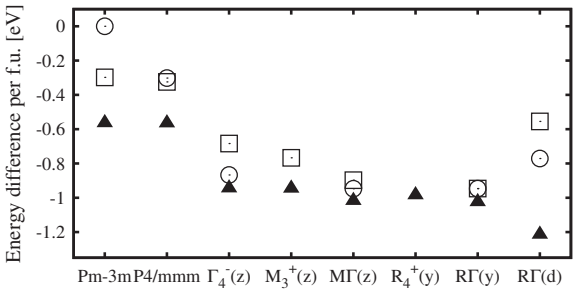

FIG. 4. Structural energetics of bulk $BiMnO_3$. Energy difference per perovskite cell (f.u.) for various structural distortions (see Fig. 3) and magnetic orderings (see Fig. 2); $P4/mmm$ corresponds to a tetragonally distorted perovskite cell with ideally positioned atoms and $M\Gamma(z)$ is a linear combination of rotational $M_3^+(z)$ and polar $\Gamma_4^-(z)$ modes.

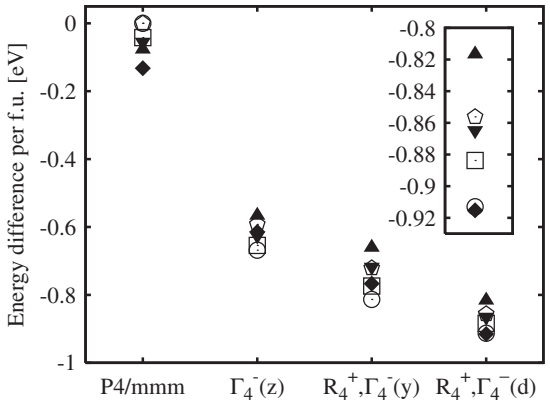

FIG. 5. Structural energetics of $BiFeO_3$-$BiMnO_3$ checkerboard. Energy difference per perovskite cell (f.u.) for different magnetic orderings (see Fig. 2) and structural distortions: (1) $P4/mmm$, (2) $\Gamma_4^-(z)$, (3) $R_4^+(y)$ and $\Gamma_4^-(y)$, (4) $R_4^+([111])$ and $\Gamma_4^-([111])$ $(R_4^+, \Gamma_4^-(d))$. Inset: zoomed view of the magnetic energies of c-$R3c$ (4) distortion.

c-$I4cm$ ground state with $R_4^+(y)$ and $\Gamma_4^-(y)$ distortions (cf. Fig. 5) the ground-state magnetic order switches from FeAFMMnFM to G-AFM, and the latter state is relatively low in energy. Switching between these two structures through application of an epitaxial strain or an electric field is thus possible, and interesting piezomagnetic and/or magnetoelectric behavior would be expected to accompany this structurally driven magnetic transition.

Experimental realization of the checkerboard would be challenging but not impossible. The formation energies of both the (001) superlattice (also reported in Ref. [22]) and the checkerboard with respect to the bulk parent compounds are positive (4 meV/f.u. and 30 meV/f.u., respectively, in the $R3c$ type of structural distortion; for the ideal perovskite structure see Table I). Indeed, as-grown Bi_2FeMnO_6 epitaxial films show no indications of cation ordering [22]. However, this does not preclude the synthesis of either of these structures under specially designed growth conditions. Both $BiFeO_3$ and $BiMnO_3$ films have been grown successfully with preferential orientations using substrate vicinality [23–25], and synthesis of (001) bilayers of $BiMnO_3$ on $BiFeO_3$ has recently been reported [26]. These techniques could be extended to produce a (110) superlattice or checkerboard. Combined state-of-the-art techniques such as patterned substration, masking, layer-by-layer growth, and careful tuning of growth parameters could potentially influence the deposition process enough to produce a $BiFeO_3$-$BiMnO_3$ structure with squares of sides down to one unit cell.

In summary, we have identified a magnetostructural effect in the atomic-scale checkerboard $BiFeO_3$-$BiMnO_3$, which is not present in either bulk or in the (001) superlattice of these two materials. We note that this behavior is due to the magnetic frustration in this system inherent to the checkerboard geometry; as a result the magnetic states are quasidegenerate and could be tuned by small perturbations including strain. Furthermore, unlike its parent compounds, the checkerboard has a multiferroic ground state with a nonzero magnetization and polarization. We remark that our first-principles calculations do not include spin-orbit coupling which is known leads to weak ferromagnetism in bulk $BiFeO_3$ [27]. The possibility of weak ferromagnetism in the antiferromagnetic phases will be pursued in future work. We also plan to investigate similar checkerboards on longer length scales, which may be easier to realize experimentally than the limiting case considered here.

We thank E. Bousquet, V. R. Cooper, M. Dawber, C.-J. Eklund, C. Fennie, A. Malashevich, M. Marsman, and D. Vanderbilt for helpful discussions. This work was supported in part by NSF MRSEC DMR-0820404, NSF NIRT-ECS-0608842, and by the U.S. Army Research Office through W911NF-07-1-0410.

[1] H. Zheng *et al.*, Science **303**, 661 (2004).
[2] S. Yeo *et al.*, Appl. Phys. Lett. **89**, 233120 (2006); C. L. Zhang *et al.*, Appl. Phys. Lett. **91**, 233110 (2007).
[3] B. S. Guiton and P. K. Davies, Nature Mater. **6**, 586 (2007).
[4] J. L. MacManus-Driscoll *et al.*, Nature Mater. **7**, 314 (2008).
[5] D. P. Kozlenko *et al.*, J. Magn. Magn. Mater. **258–259**, 290 (2003).
[6] T. Murata *et al.*, J. Magn. Magn. Mater. **310**, 1555 (2007).
[7] C. J. Fennie and K. M. Rabe, Phys. Rev. Lett. **97**, 267602 (2006).
[8] R. T. Lechner *et al.*, Phys. Rev. Lett. **94**, 157201 (2005).
[9] G. Kresse and J. Furthmuller, Phys. Rev. B **54**, 11 169 (1996).
[10] A. I. Liechtenstein, V. I. Anisimov, and J. Zaanen, Phys. Rev. B **52**, R5467 (1995).
[11] S. L. Dudarev *et al.*, Phys. Rev. B **57**, 1505 (1998).
[12] J. B. Neaton *et al.*, Phys. Rev. B **71**, 014113 (2005).
[13] P. Baettig *et al.*, J. Am. Chem. Soc. **129**, 9854 (2007).
[14] P. E. Blochl, Phys. Rev. B **50**, 17 953 (1994).
[15] G. Kresse and D. Joubert, Phys. Rev. B **59**, 1758 (1999).
[16] H. J. Monkhorst and J. D. Pack, Phys. Rev. B **13**, 5188 (1976).
[17] R. D. King-Smith and D. Vanderbilt, Phys. Rev. B **47**, 1651 (1993).
[18] L. Pálová, P. Chandra, and K. M. Rabe (to be published).
[19] H. T. Stokes *et al.*, Acta Crystallogr. Sect. B **58**, 934 (2002).
[20] C. Michel *et al.*, Solid State Commun. **7**, 701 (1969).
[21] A. A. Belik *et al.*, J. Am. Chem. Soc. **129**, 971 (2007).
[22] L. Bi *et al.*, Phys. Rev. B **78**, 104106 (2008).
[23] Y.-H. Chu *et al.*, Adv. Mater. **19**, 2662 (2007).
[24] J. Li *et al.*, Appl. Phys. Lett. **84**, 5261 (2004).
[25] J. Y. Son and Y.-H. Shin, Appl. Phys. Lett. **93**, 062902 (2008).
[26] C.-H. Yang *et al.*, J. Korean Phys. Soc. **55**, 80 (2009).
[27] C. Ederer and N. A. Spaldin, Phys. Rev. B **71**, 060401(R) (2005).